福井大学リポジトリ
UFR
UNIVERSITY OF FUKUI REPOSITORY

Mapping of a Ni/SiNx/n-SiC structure using scanning internal photoemission microscopy

メタデータ	言語: eng 出版者: 公開日: 2019-04-02 キーワード (Ja): キーワード (En): 作成者: Kenji, Shiojima, Takanori, Hashizume, Masaru, Sato, Mayumi, B Takeyama メールアドレス: 所属:
URL	http://hdl.handle.net/10098/10597

Copyright (C) 2019 The Japan Society of Applied Physics

Mapping of Ni/SiN_x/n-SiC structure using scanning internal photoemission microscopy

Kenji Shiojima[1]*, Takanori Hashizume[1], Masaru Sato[2], and Mayumi B. Takeyama[2]

[1] *Graduate School of Electrical and Electronics Engineering, University of Fukui, Fukui 910-8507, Japan*

[2] *School of Earth, Energy and Environmental Engineering, Faculty of Engineering, Kitami Institute of Technology,*
Kitami, Hokkaido 090-8507, Japan

*E-mail: shiojima@u-fukui.ac.jp

SiN_x films formed on n-SiC layers have been characterized by using scanning internal photoemission microscopy (SIPM) in metal-insulator-semiconductor diode structure. After applying forward-biased voltage stress up to 30 V, the diode was partially degraded. SIPM clearly imaged the degradation pattern with a large photocurrent, which consisted with the microscopy image. These results clarified that the partial degradation induced a leak path with a low energy barrier.

1. Introduction

We have developed a new two-dimensional mapping characterization termed scanning internal photoemission microscopy (SIPM) to verify the electrical inhomogeneity of metal-semiconductor (M/S) interfaces.[1, 2] Thus far, we have demonstrated the mapping of characteristics in interfacial reactions, degradation under applying voltage stress and surface damage in Si, GaAs, GaN, IGZO, and SiC Schottky contacts.[3-10] We also demonstrated the characterization of crystal quality of wafer-bonded Si/SiC heterointerfaces.[11] We confirmed that macroscopic mapping investigation for the entire electrodes by using this technique is a powerful tool for developing high-power wide-bandgap electron devices.

We set metal/insulator/semiconductor (MIS) structure as a next target for SIPM. Thermally oxidized SiO_2 films on Si and SiC, and SiN and SiO_2 films formed by chemical vapour deposition are intensively studied for MIS structure for many years including process techniques, device performances and reliability. On the other hand, with the recent decrease in process temperature, a technique of depositing an insulating film at low temperatures attracts attention. In particular, growing interest in SiN_x films of high density has given an impetus to the development of low-temperature deposition of the films with reduced hydrogen content [12-14] in solar cell applications and the through Silicon Via in three-dimensional integration, and the passivation layer on various devices such as memories, light-emitting devices, and display devices.[15-17] The SiN_x films have been prepared by plasma-enhanced chemical vapor deposition (PECVD) using silane and ammonia reactants.[18-20] However, there is a problem that a large amount of hydrogen (20-40 at.%) incorporation in the PECVD SiN_x films.[21] On the other hand, many researchers have examined characteristics of the SiN_x films deposited by reactive sputtering in recent years.[22-25] Takeyama et al., obtained the reactively sputtered SiN_x films with a high density, high refractive index, and low hydrogen content at low deposition temperatures.[22] However, the evaluation of electrical characteristics of these sputtered SiN_x films is still insufficient. In this study, we examine the breakdown by the application of high voltage by using the sputtered SiN_x films at two-dimensionally evaluation.

Since SIPM is based on the internal photoemission effect, photoresponse (PR) measurement, in conventional Schottky contacts and heterojunctions, carriers can go through the M/S or semiconductor-semiconductor (S/S) interfaces upon irradiation a monochromatic light with photon energy (hv), exceeding energy discontinuity (ΔE) at the interfaces and below energy bandgap (E_g) of the semiconductor, which is typically below 3 eV.[5, 11] This carrier transport across the interface generates a photocurrent (true current) by this mechanism. When we investigate metal/insulator (SiO_2, Al_2O_3) /semiconductor (Si, SiC) (MIS) structure with the internal photoemission effect, a monochromatic light with hv> 3 eV is conventionally used, as ΔE at the M/I and I/S interfaces is so large.[26, 27] In our previous report, we deposited SiN_x films by RF reactive sputtering on chemically stable SiC substrates to form MIS structure, and found that in the SIPM measurements, photocurrents were successfully detected even with a green (hv = 2.40 eV) laser.[28] In this paper, we report in more detail photocurrent transport mechanism and the initial stage of the degradation in this structure.

2. Device fabrication and measurement

Figure 1 shows the device structure of the Ni/SiN_x/SiC MIS contact. A 9.73-μm-thick n-SiC (n: 1.2×10^{16} cm^{-3}) layer was grown on a 4H-n-SiC substrate. Then, in the other sputtering chamber, the Si target was pretreated with an Ar + H_2 gas mixture to eliminate surface contaminants, as reported elsewhere.[22, 23] 50- or 20-nm-thick SiN_x layers were deposited by RF reactive sputtering using pure Si target (2 inches in diameter) and Ar + N_2 (+H_2) gas mixture. The substrate temperature was set within a range from room temperature to 400 ° C. Circular 100-nm-thick Ni contacts (200 μm in diameter) were deposited on the SiN_x surface by the electron beam evaporation. After that, InGa ohmic contacts were deposited on the back surface.

We performed current-voltage (I-V) and capacitance-voltage (C-V) measurements using a semiconductor parameter analyser and an LCR meter at 1 MHz, respectively, in order to investigate basic electrical characteristics. The forward I-V measurements also act as application of voltage stress to investigate device degradation. Prior to the SIPM measurements, we also conducted conventional PR measurements, where hv was continuously scanned from 1.2 to 4.0 eV, in order to confirm the shape of the PR

spectrum of the Ni/SiN_x/n-SiC structure. In this measurement, a monochromatic light from a monochrometer was used and irradiated to the entire contact area. The photocurrent was detected with a lock-in amplifier. We define photoyield (Y) as a photocurrent per incident photon.

SIPM measurement was conducted basically in the same manner as in our previous report.[5] In the SIPM measurements, one focuses and scans the beam over the interface of one electrode to obtain a two-dimensional image of Y. Green (λ = 517 nm, $h\nu$ = 2.40 eV) laser was used in this SIPM measurement. The diameter of the laser beam was less than 2 μm.

3. Results and discussion

3.1 Basic electrical characteristics

We show in Fig. 2(a) the reverse I-V characteristics of the samples with the 20- and 50-nm-thick SiN_x layers. For both samples the reverse biased currents gradually increased up to 30 μA at V = -100 V without break-down. The SiN_x layers are basically insulator, however, as the thicknesses are thin, a certain level of leakage currents were detected.

In the lower voltage range of the forward I-V characteristics as shown in Fig. 2(b), the currents around 10 pA can be seen for the both samples. The currents increased sharply at around 13 and 20 V for the samples with the 20- and 50-nm-thick SiN_x layers, respectively. These are symptoms of the degradation. The estimated break-down field of the SiN_x layer is roughly 2 MV/cm. After the degradation, in these measurements, the voltage was continuously applied up to 30 V and the currents were kept flowing at 10 mA, which is a maximum limit of the semiconductor parameter analyser. After the measurements, the electrical characteristics of the both samples became short.

Before the degradation during the I-V measurements, we conducted C-V measurements with reverse biased voltage sweeps from 0 to -40 V and from -40 to 0 V as shown in Fig. 3. The C values are almost the same and constant at 8.6 pF under the applied voltage from 0 V to -8 V for the 20-nm sample and to -20 V for the 50-nm sample. Supposing the MIS band diagram is in accumulation, the C value should depend on the thickness of the insulator. In addition, the estimated accumulation C value with the reported

dielectric constant of 7.5 for Si_3N_4 is 40 pF.[29] We are not sure the dielectric constant of our SiN_x film, but this value is much larger than our measured one. One reason is due to strong Fermi-level pinning the junction is not in the accumulation, the total *C* consists of a series connection of the SiN_x layer and depletion layer of SiC. The depletion layer *C* would be dominant. Another reason is that the SiN_x layer *C* may have measurement frequency dispersion. In our measurement frequency at 1MHz, *C* may be under estimated. Under further deep reverse biased voltage, the *C* values gradually decreased less than 3 pF down to -40 V, and slight hysteresis was observed for the both samples. These behaviours are a typical deep-depletion, and the thickness of the SiN_x layer is affected to the threshold voltage.

Conventional PR measurements were conducted, where a monochromatic light was illuminated over the entire contact. Figure 4 shows the entire PR spectra for the both samples. In the almost all *hv* range, photocurrent was detected. As mentioned in the introduction section, in this relatively small *hv* range, the photocurrent with carrier transport (true current) is not expected due to a large energy discontinuity in the MIS structure. We consider that a total current (*I*) consists of true (*i*) and displacement ($\frac{\partial D}{\partial t}$, where *D* is electric flux density and ρ is charge density) currents based on the electromagnetism theory,

$$\mathrm{I} = \mathrm{i} + \frac{\partial D}{\partial t}, \tag{1}$$

$$\rho = div\, D. \tag{2}$$

As long as we use lock-in detection for the photocurrent, displacement current resulted from variation of charge distribution upon irradiation is expected. When the *hv* range is from 1.2 to 2.5 eV, *Y* was small and monotonically increased with with an on-set energy of 1.0 eV. The origin is not clear at this moment, but the interfacial states at the SiN_x/SiC is possible. Then, we found a peak at *hv*= 2.7 eV. This energy position is in a good agreement with D-A pair luminescence in 4H-SiC.[30] When *hv*>3.2 eV, large *Y* signals were detected. This is owing to the fundamental absorption in 4H-SiC (E_g=3.2 eV), which generates electron-hole pairs. Above *hv*=3.5 eV, *Y* dropped, because the 4H-SiC substrate is sufficiently thick to absorb the incident light. In the entire *hv* range, the *Y* intensity of the sample with the 20-nm-thick SiN_x layer is larger than that of the 50-nm sample. The thinner SiN_x layer might induce larger *D* in the MIS structure. These PR

spectra also tell us that, in the SIPM measurements, the green laser can generate current in this MIS structure.

3.2 Mapping characterization

Figure 5 shows typical optical microscopy images and *Y* maps with green laser of the sample with the 50-nm SiN_x layer. Before the forward voltage stress to 30 V, (a) the electrode surface in the microscopy image is flat. However, (b) in the *Y* map, *Y* is largest in the center of the electrode and gradually decreased to the periphery like a bell shape. Moreover, the edge of the electrode is not clear. This is completely different from the maps of M/S interfaces, which we have reported so far.[5] In the case of Schottky contacts, *Y* is uniform and the edge is clearly observed in the special resolution defined by the laser beam diameter at the interface of less than 2 μm. In order to explain this unusual result, we conducted additional mapping experiments in different dot diameter and lock-in reference frequency for both this MIS and conventional Ni/n-SiC Schottky electrodes. For the Schottky contacts, the same *Y* value was obtained even we change the dot diameter and the reference frequency. On the other hand, for the MIS, when we change the dot diameter from 200 to 300 μm, *Y* increased 1.7 times. When we change the reference frequency from 83 to 166 Hz, *Y* increased 1.3 times. These results indicate that the displacement current is responsible for this unusual result, because the larger *C* and higher frequency can enhance the displacement current. In this MIS structure, the M/I interface is defined by metal dot pattern, but the I-S interface has a large area (the SiN_x layer was not mesa-etched). The variation of the charge by light irradiation can spread out along the I/S interface.

After the degradation, (c) in some portions the surface morphology of the electrode became rough in the microscopy image. Probably these regions were formed by the voltage stress. In (d) the green *Y* map, the shape of the degraded regions was clearly visualized as observed in the optical microscopy image. *Y* in the degraded regions increased 2-3 times than that in the flat region (notice that the *Y* scale is 2.7 times larger than that in (b)), and the phase difference in the lock-in detection changed by 40°. The insulator broke and a leakage path with a lower energy barrier was formed by the voltage stress. As a result of that, a photocurrent with a true-current component was generated.

3.3 Initial stage of the degradation

During the forward *I-V* measurements as shown in Fig. 2(b), the significant degradation occurred. Therefore, we conducted a forward-voltage sweep three times with increasing a compliance current of 1×10^{-5}, 1×10^{-3}, and 1×10^{-2} A for the sample with the 20-nm SiN_x layer, in order to investigate the initial stage of the degradation. At the same time as the current reached the compliance, the applied voltage was shut off. For the first sweep as shown in Fig. 6, the current steeply increased at 4.8 V. Then, for the second and third sweeps, the current level increased in turn. We found that the degradation gradually proceeded by each sweep. In the optical microscopy image of the dot in Fig. 7(a), no symptom of the degradation was observed even after the third sweep. In the SIPM results, the *Y* was fairly uniform over the dot after the first sweep as shown in Fig. 7(b). After the second sweep, however, we find some spots standing out from the uniform region. Within the spots, *Y* is about 1.4 times as large as that in the other region. After third sweep, the number of the spots increased. Therefore, we demonstrated that SIPM clearly visualized an initial stage of the degradation sensitively in conjunction with the electrical characteristics.

4. Conclusions

SIPM measurements were applied to map the degradation of the RF reactive sputtered SiN_x layers in SiC MIS structure. After application of the voltage stress up to 30 V, partial degradations were clearly visualized in the SIPM *Y* maps. The SiN_x insulator broke and a leakage path with a lower energy barrier was formed by the voltage stress. We found that this method is a powerful tool to investigate symptoms of the degradation of the MIS structure.

Acknowledgment

A part of this work was supported by a Grant-in-Aid for Scientific Research C 18K04228 and 15K05975of the Ministry of Education, Culture, Sports, Science and Technology.

References

1) T. Okumura and K. Shiojima, Jpn. J. Appl. Phys. **28**, 1108 (1989).
2) K. Shiojima and T. Okumura, Jpn. J. Appl. Phys. **30**, 2127 (1991).
3) K. Shiojima and T. Okumura, J. Cryst. Growth **103**, 234 (1990).
4) K. Shiojima and T. Okumura, Proc. 29th Annu. Int. Reliability Physics Symp. 1991, p. 234.
5) K. Shiojima, S. Yamamoto, Y. Kihara, and T. Mishima, Appl. Phys. Express **8**, 046502 (2015).
6) S. Yamamoto, Y. Kihara, and K. Shiojima, Phys. Status Solidi B **252**, 1017 (2015).
7) K. Shiojima, S. Murase, S. Yamamoto, T. Mishima, and T. Nakamura, Jpn. J. Appl. Phys. **55**, 04EG05 (2016).
8) K. Shiojima and M. Shingo, Phys. Status Solidi B **254**, 1600587 (2017).
9) S. Murase, T. Mishima, T. Nakamura, and K. Shiojima, Mater. Sci. Semicond. Process. **70**, 86 (2017).
10) A. Terano, H. Imadate, K. Shiojima, Materials Science in Semiconductor Processing, **70**, 92 (2017).
11) M. Shingo, J. Liang, N. Shigekawa, M. Arai, and K. Shiojima, Jpn. J. Appl. Phys. **55**, 04ER15 (2016).
12) R. B. Fair and R. C. Sun, IEEE Trans. Electron Devices **28**, 83 (1981).
13) S.-S. Han, B.-H. Jun, K. No, and B.-S. Bae, J. Electrochem. Soc. **145**, 652 (1998).
14) S. Ueno, M. Suzuki, Y. Konishi, and K. Azuma, Japan Patent W02012/029709 A1 (2012).
15) D. Li, F. Wang, D. Yang, and D. Que, Optics Express **20**, 17360 (2012).
16) A. Sato, M. Shimada, K. Abe, R. Hayashi, H. Kumomi, K.Nomura, T. Kamiya, M. Hirano, and H. Hosono, Thin Solid Films **518**, 1309.
17) H. Kitada, N. Maeda, K. Fujimoto, Y. Mizushima, Y. Nakata, T. Nakamura, and T. Ohba, Jpn. J. Appl. Phys. **50**, 05ED02 (2011).
18) E. Herth, B. Legend, L. Buchaillot, N. Rolland, and T. Lasri, Microelectron. Reliab. **50**, 1103 (2010).
19) M. C. Wei, S. J. Chang, C. Y. Tsia, C. H. Liu, and S. C. Chen, Sol. Energy **80**, 215 (2006).

20) M. Orfert and K. Richter, Surf. Coatings Technol., **622,** 116 (1999).
21) G. Lucovsky and D. V. Tsu, J. Vac. Sci. Technol. **5**, 2231 (1987).
22) M. B. Takeyama, M. Sato, Y. Nakata, Y. Kobayashi, T. Nakamura, and A. Noya, Jpn. J. Appl. Phys. **53**, 05GE01 (2014).
23) M. Sato, M. B. Takeyama, Y. Nakata, Y. Kobayashi, T. Nakamura, and A. Noya, Jpn. J. Appl. Phys. **55**, 04EC05 (2016).
24) F. Henry, C. Y. Duluard, A.Batan, and F. Reniers, Thin Solid Films **520**, 6386 (2012).
25) G. Sombrio, P. L. Franzen, R. L. Maltez, L. G. Matos, M. B. Pereira, and H. Boudinov, J. Phys. D **46**, 235106 (2013).
26) V. Afanas'ev, F. Ciobanu, S. Dimitrijev, G. Pensl, and A. Stesmans, J. Phys. Condens. Matter. **16**, S1839 (2004).
27) V. Afanas'ev, and A. Stesmans, Appl. Phys. Lett. **77**, 2024 (2000).
28) K. Shiojima, T. Hashizume, M. Sato, and M. B. Takeyama, Ext. Abstr. Int. Conf. Solid State Devices and Materials (SSDM2018), 2018, PS-3-07.
29) S. M. Sze, *Physics of Semiconductor Devices* (Wiley, New York, 1981) 2nd ed., p. 852.
30) M. Ikeda, H. Matsunami, and T. Tanaka, Phy. Rev. B **22**, 2842 (1980).

Figure Captions

Fig. 1. (Color online) Device structure of the Ni/SiN_x/SiC MIS contact.

Fig. 2. (Color online) (a) Reverse and (b) forward *I-V* characteristics of the samples with the 20- and 50-nm-thick SiN_x layers.

Fig. 3. (Color online) *C-V* characteristics with reverse biased voltage sweeps from 0 to -40 V and from -40 to 0 V.

Fig. 4. (Color online) Typical PR spectra in a $Y^{1/2}$ vs hv plot.

Fig. 5. (Color online) Optical microscope images of the Ni electrode surfaces (a) before and (c) after the voltage stress up to +30 V and *Y* maps measured using the green laser (b) before and (d) after the stress.

Fig. 6. (Color online) Forward *I-V* characteristics during three voltage sweeps with increasing a compliance current of 1×10^{-5}, 1×10^{-3}, and 1×10^{-2} A.

Fig. 7. (Color online) (a) Optical microscope images of the Ni electrode surfaces after the voltage sweep with the compliance current of 1×10^{-2} A, and *Y* maps after the sweep with the compliance current of (b) 1×10^{-5}, (c) 1×10^{-3}, and (d) 1×10^{-2} A.

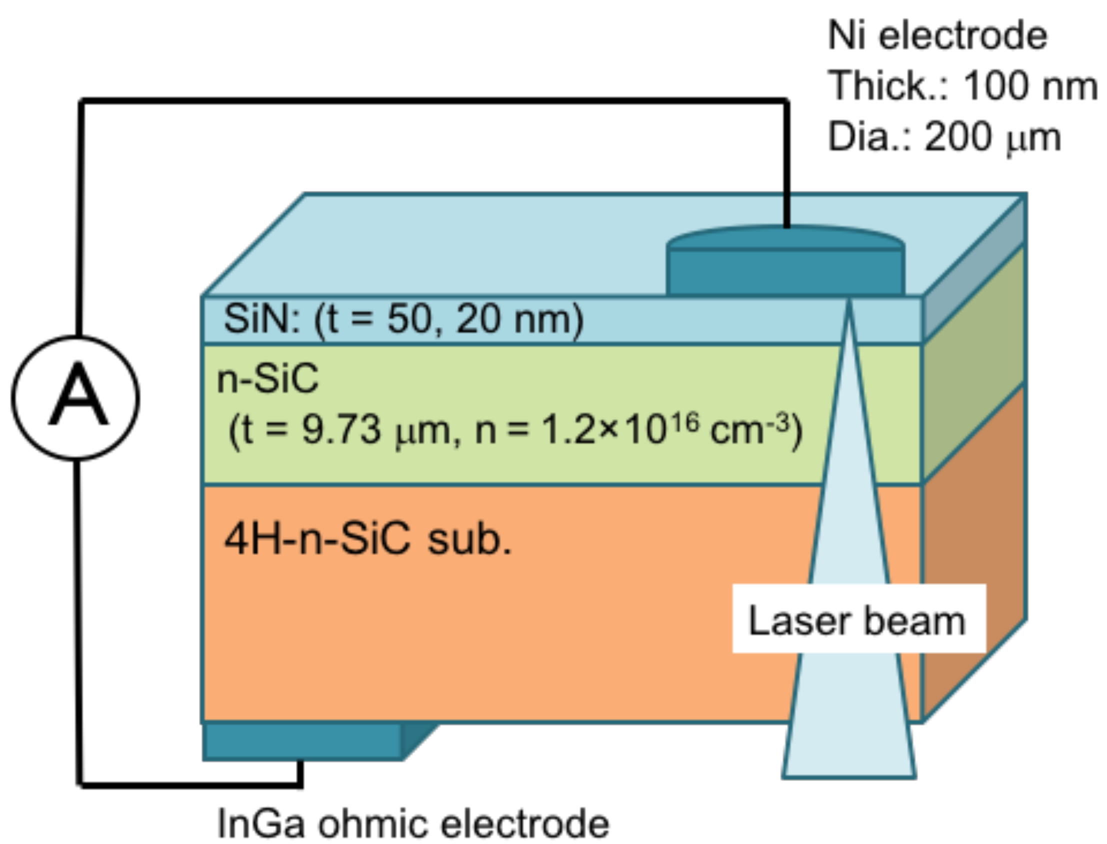

Fig. 1

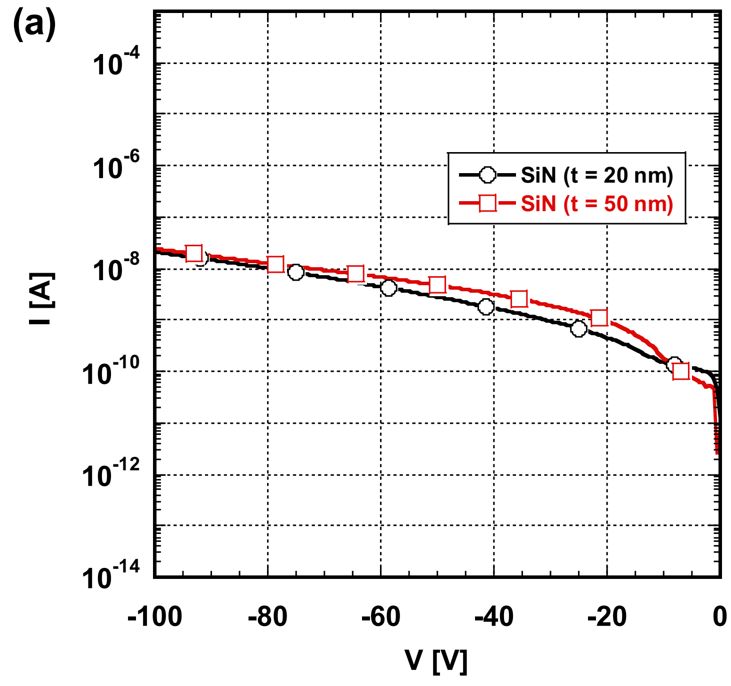

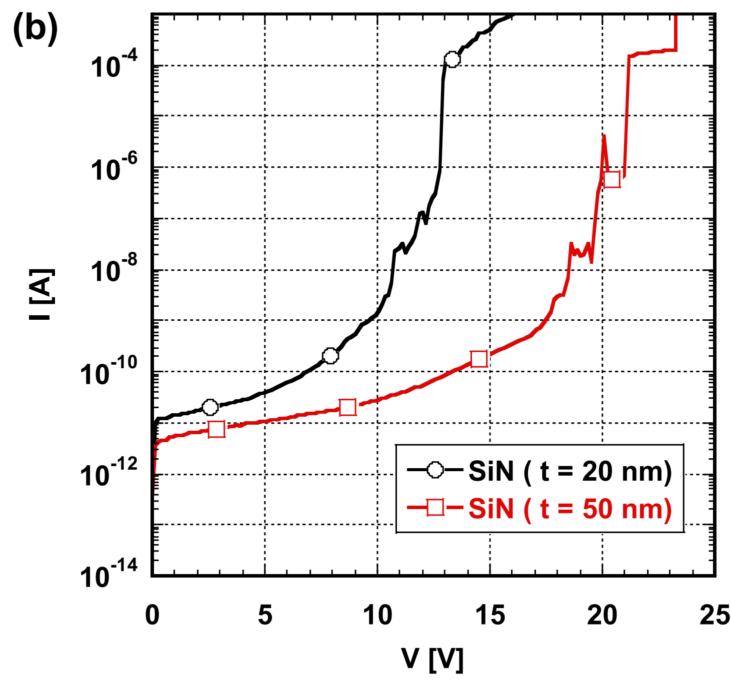

Fig. 2

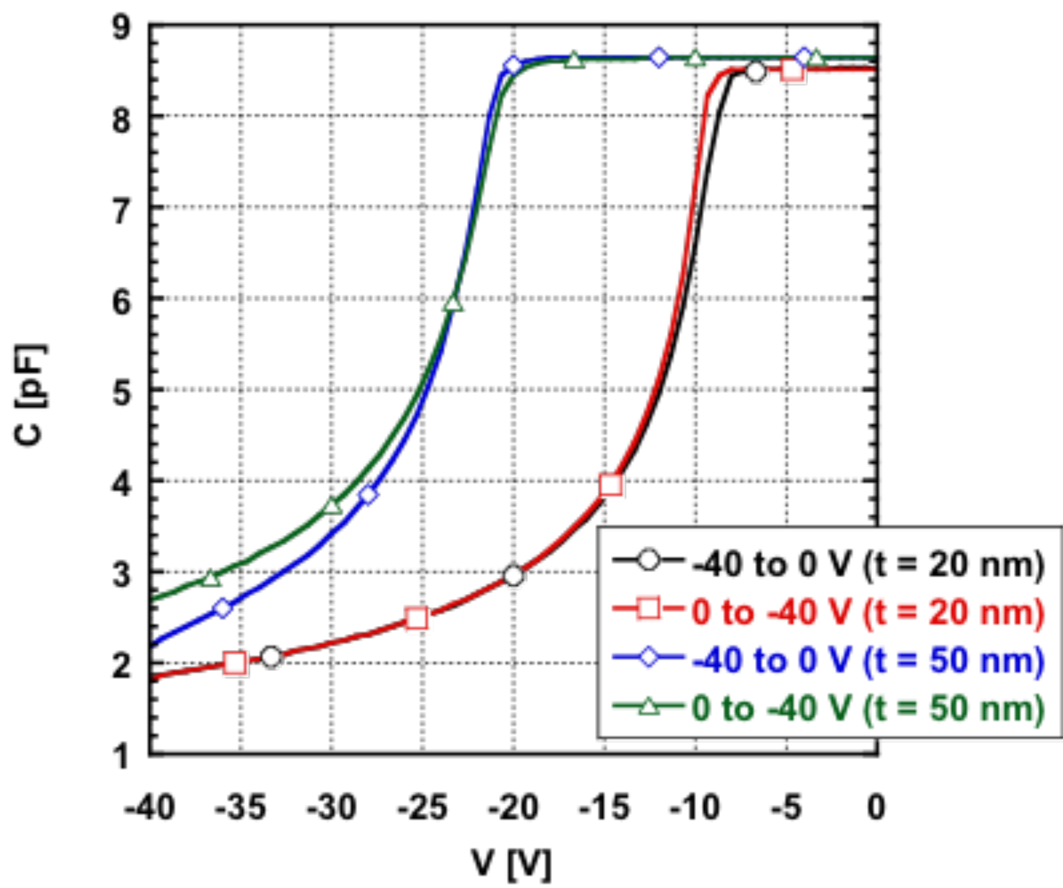

Fig. 3

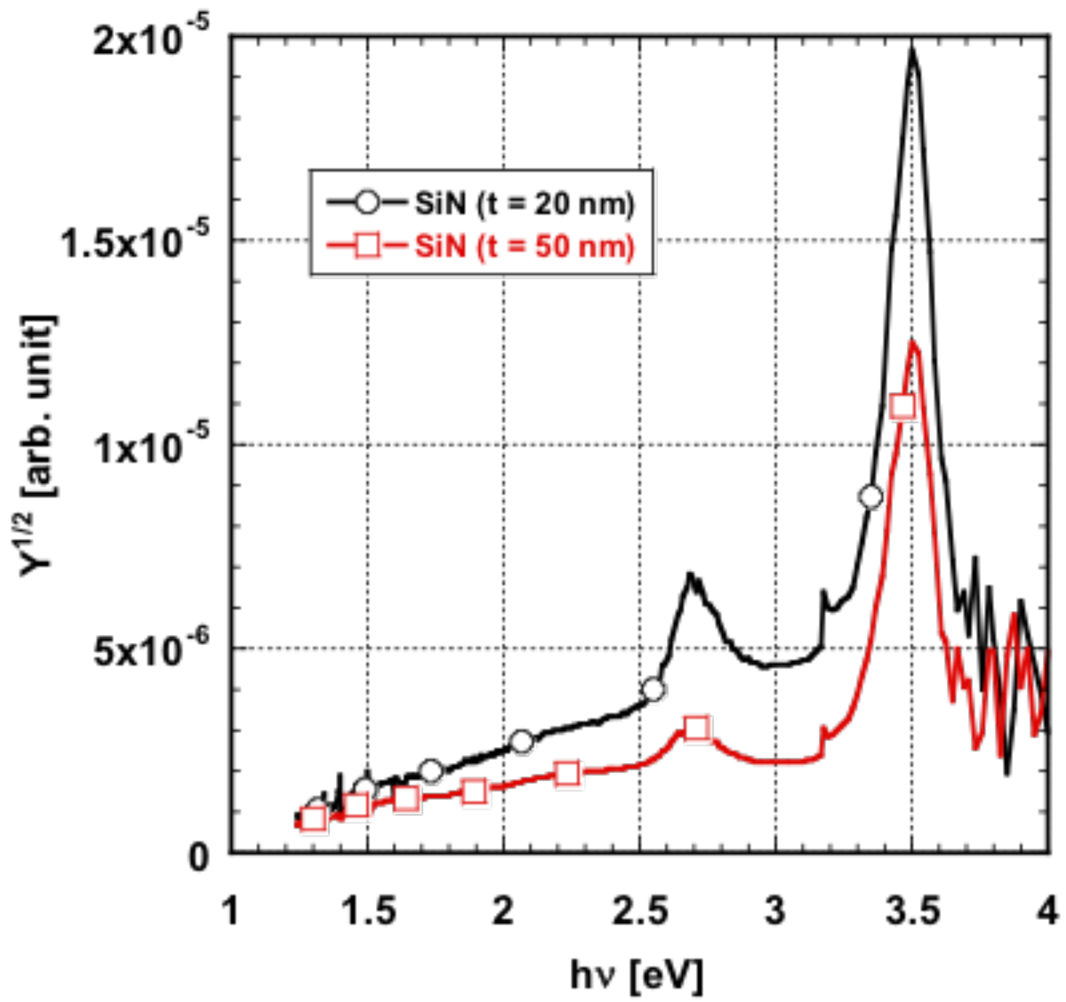

Fig. 4

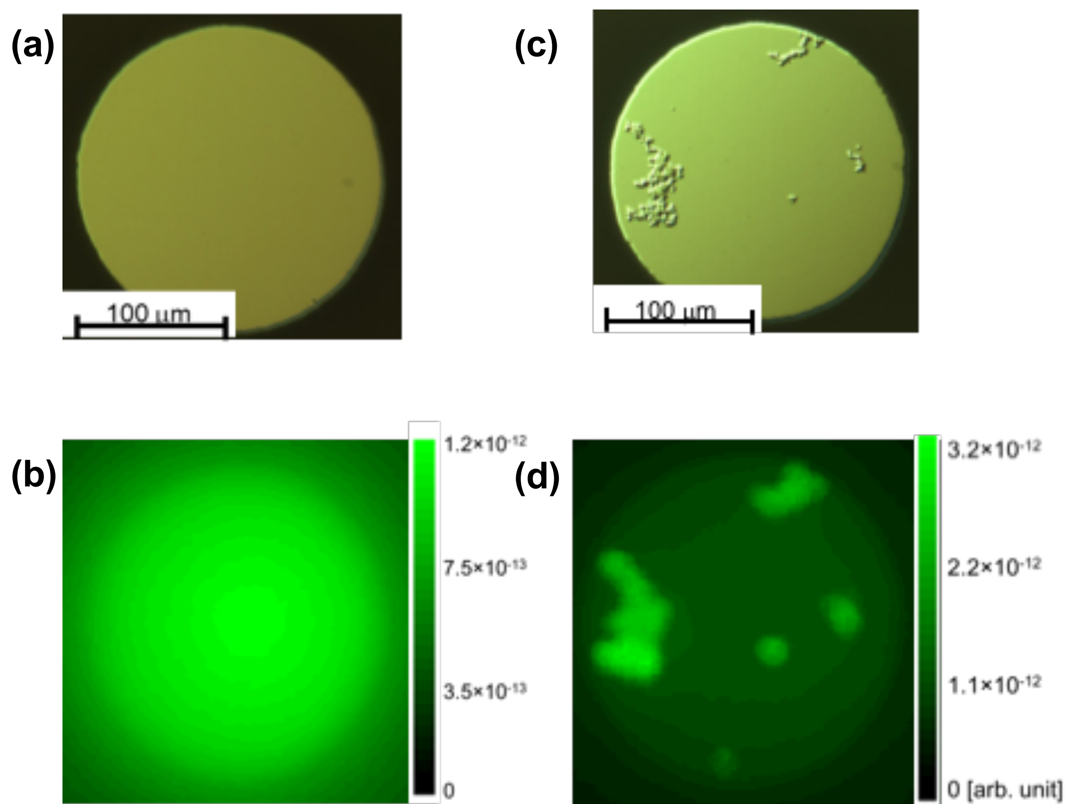

Fig. 5

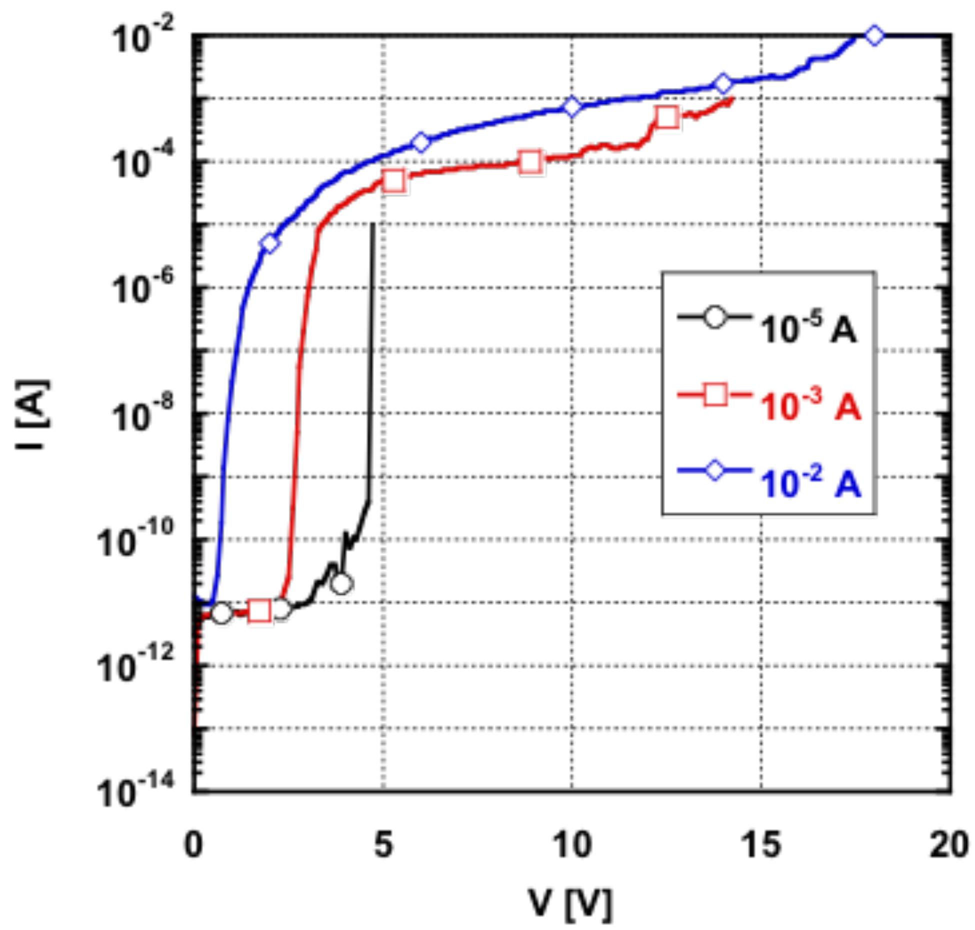

Fig. 6

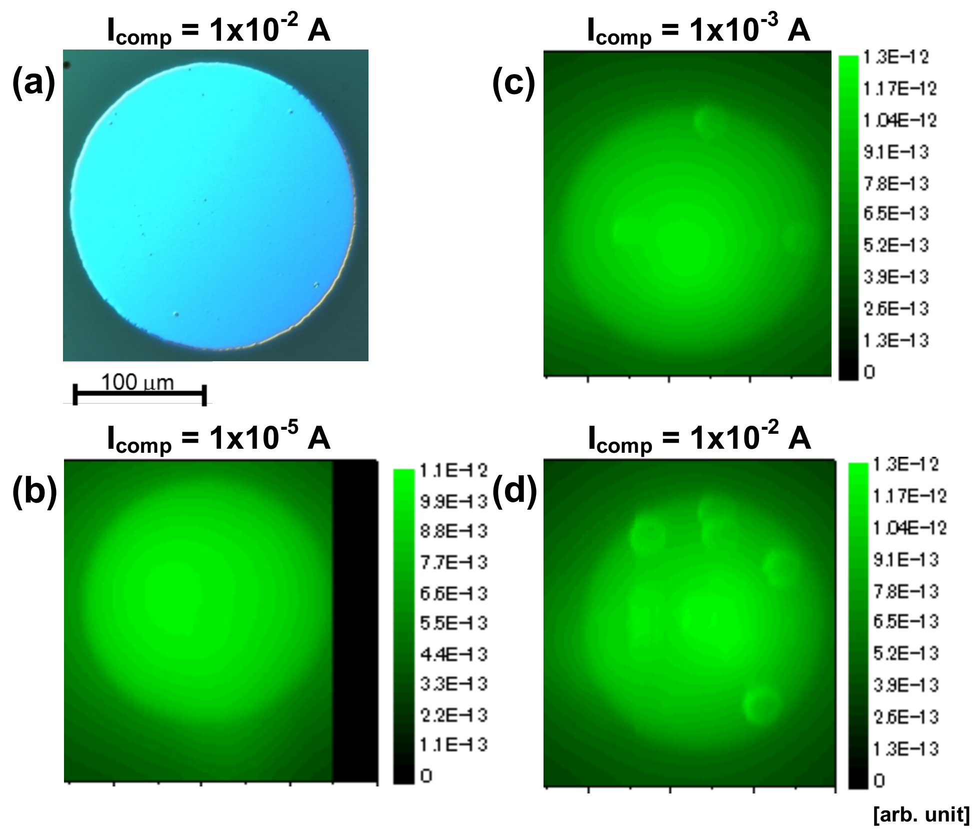

Fig. 7